EUROPEAN COOPERATION
IN THE FIELD OF SCIENTIFIC
AND TECHNICAL RESEARCH

EURO-COST

SOURCE: Signal Processing and Speech Communication
Laboratory, Graz University of Technology, Austria

COST IC1004 TD(11)01014
Lund, Sweden
June 20-21, 2011

Indoor UWB Channel Analysis in an Atrium-Style Office Building for Multipath-Aided Localization

Paul Meissner, Daniel Arnitz, Thomas Gigl and Klaus Witrisal
Inffeldgasse 16c
A-8010 Graz
Austria
Phone: +43 316 873 4363
Fax: +43 316 873 104363
Email: paul.meissner@tugraz.at, witrisal@tugraz.at

Indoor UWB Channel Analysis in an Atrium-Style Office Building for Multipath-Aided Localization

Paul Meissner, Daniel Arnitz, Thomas Gigl and Klaus Witrisal
Graz University of Technology, Graz, Austria, Email: {paul.meissner, daniel.arnitz, thomas.gigl, witrisal}@tugraz.at

***Abstract*—We present a detailed analysis of an indoor UWB channel measurement campaign. The focus is on the modeling of the deterministic part of the multipath channel using a-priori known relevant reflections and scatterers, found from an available floor plan. Our approach uses virtual signal sources, whose locations and visibilities can be calculated using simple ray-launching techniques. The channel analysis steps exploit these results, using an effective multipath cancellation method that introduces virtually no artifacts. We show that the corresponding multipath-components can explain up to 90 % of the UWB channel impulse responses in terms of energy capture. This is important for multipath-aided indoor localization, which provides robust position fixes using a single base station only.**

I. Introduction

For indoor localization, time-of-arrival (ToA) based systems using (ultra)-wideband (UWB) signals are favorable, due to their fine delay resolution. In indoor scenarios, the large number of interacting objects like walls or furniture usually results in dense multipath channels, i.e. the channel impulse response (CIR) at a specific position consists of many specular reflections as well as diffuse scattered components [1]. If a floor plan is available, signal paths reflected of the room walls can be mapped to virtual signal sources [2], which are mirror images of the base station with respect to the corresponding reflecting surface, so-called *virtual anchors* (VAs). Using statistical models for range estimates to these virtual nodes, we have achieved robust algorithms for indoor localization and tracking in [3].

This contribution presents the results of a recently performed indoor UWB channel measurement campaign. Our localization algorithms are based on the fact that the UWB channel gives access to the specular reflections associated to the geometry of virtual sources [4]. It is important to know if these, usually few, expected multipath-components (MPCs) are important features of the channel and if they can be identified. We answer the former question by cancelling these expected MPCs from the CIRs obtained in our measurements with a time-domain method, i.e. a search-and-subtract approach [5]. A multipath template signal is generated at a position within a room with the help of the known distances to the virtual sources [2]. In the method presented in this paper, an additional pulse-shaping step is proposed that reduces artifacts of the MPC-cancellation. The amount of energy contained in the cancelled MPCs can be quantified by energy capture, which is also an important measure for the design of Rake receivers [6]. We show that using the few expected reflections allows for a large fraction of the energy to be accounted for. In comparison to other results in the literature, e.g. [7], we achieve high energy capture values for relatively low numbers of considered MPCs. This shows that geometry and position-related prior information can make search-and-subtract approaches very effective.

The approach presented here has some similarities to ray-tracing, which is a valuable, but computationally demanding tool in both localization and channel analysis [8]. Our aim is a complexity tradeoff: We do not use ray-tracing techniques to accurately predict amplitudes and delays of possible signal paths at a specific location, but rather use it beforehand to compute and investigate potential reflectors and scatterers.

The rest of this paper is organized as follows: Section II describes the measurement campaign and the geometric computations that are needed. In Section III we describe the channel analysis and MPC cancellation method. Results are discussed in Section IV and Section V draws conclusions.

II. Measurement and geometric modeling

Our measurement campaign was motivated by the intended application of indoor localization and tracking of a moving agent, as described in [3]. To this end, we measured the UWB channel between a mobile station and six base stations along an example trajectory as can be seen in Fig. 1. This route consists of 381 points with a spacing of $10\,\text{cm}$, covering a total distance of $38\,\text{m}$. The measurements were performed in the frequency domain using a Rhode & Schwarz ZVA-24 vector network analyzer. At each position k, the complex channel transfer function $H_k(f)$ is measured at 7501 frequency points over the frequency range from 3.1 to 10.6 GHz. This results in a maximum resolvable delay of approx. $1\,\mu\text{s}$ (or approx. $300\,\text{m}$ path delay), and a delay resolution of $0.133\,\text{ns}$ (or $4\,\text{cm}$ path resolution). In performance evaluations, we will also restrict the bandwidth to $2\,\text{GHz}$ (the range from $6-8\,\text{GHz}$), resulting in a delay resolution of $0.5\,\text{ns}$ (or $15\,\text{cm}$ path resolution).

The measurement location is the ground floor of our lab. This is an atrium style hallway of an office building, whose outer walls, marked with black lines in the floor plan, are made of concrete. Concerning geometry and building

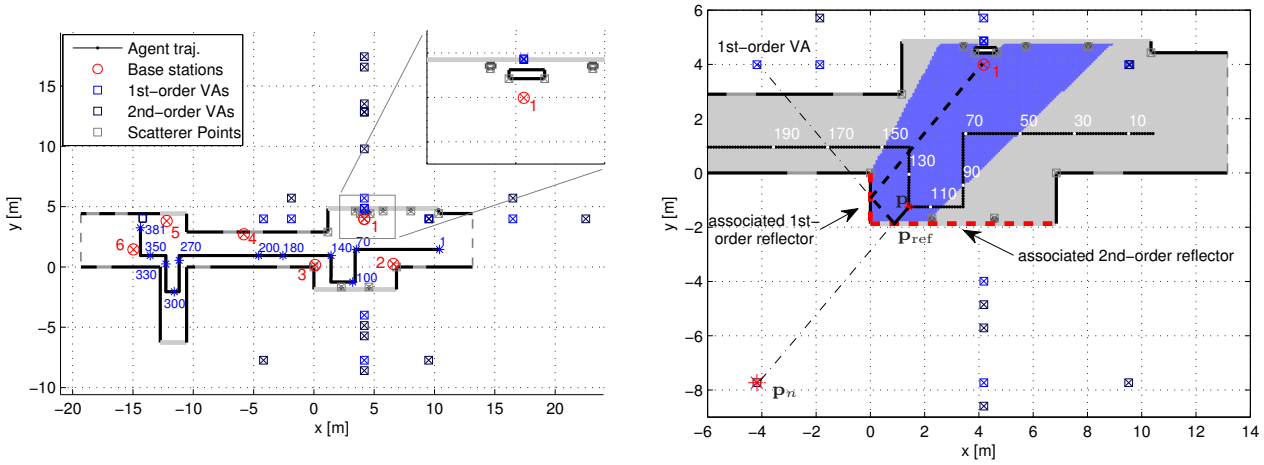

Fig. 1. Left plot shows floor plan, agent trajectory and base stations (BS) for the measurement scenario. Also shown are considered virtual anchors (VAs) for BS 1. The right plot shows an example for the calculated expected visibility region (in blue) of a specific second-order VA of BS 1 together with its associated reflecting surfaces (marked in red). Also shown is an example signal path (dashed black line, dash-dotted lines indicate "virtual paths" to the VAs) from point $\mathbf{p}$ to the BS. Indices of some trajectory points are given for orientation, as they are occasionally used in the text.

materials, the environment could be classified as semi-industrial. As can be seen in the floor plan, there are large reflective windows in the area of the initial part of the trajectory, shown as grey lines in the floor plan. Inbetween these windows are narrow metal pillars, which we expect to be visible as point scatterers (see also the zoom in Fig. 1). Doors are made of metal and also shown as grey line segments. The building consists of three floors, which are not separated by ceilings. Nevertheless, there are bridges connecting the two sides on the upper floors, which consist of both concrete and metal. The dashed lines at the right and left side of the floor plan are just delimiting the area we take into account for analysis. The building extends several meters to the right and several tens of meters to the left. Stationary channel conditions were ensured during the measurements.

TABLE I
MEASUREMENT PARAMETERS

Parameter	Value	Comment
Frequency range	$3.1 - 10.6\,\mathrm{GHz}$	full measurement BW
	$6 - 8\,\mathrm{GHz}$	offline bandlimitation
Trajectory parameters	381 points	
	10 cm spacing	
Frequency points	7501	over full bandwidth

For the moving agent, we used a Skycross SMT-3TO10M UWB antenna. Also two of the BSs used an antenna of this type (BS 3 and 4), the other ones used a custom-made coin antenna, made of two 5 Euro-cent coins [9]. Both antenna types have approximately uniform horizontal gain patterns. For all BSs as well as the moving agent, the antennas were mounted on a tripod, at a height of 1.5 m. Floor plan, as well as agent and base station positions, were measured manually using a laser distance meter.

Having the floor plan and the positions of the BSs available, we can compute the possible positions of VAs. For first-order wall reflections, the VAs are simply mirror images of the BS at the corresponding reflective surface, which we call the associated reflector. Second-order VAs can be obtained by mirroring the first-order VAs at the associated second-order reflectors. Although this procedure can be repeated for higher orders, we restrict ourselves to VAs up to second-order in this work. Another model restriction is given by the 2D-modeling. Although the environment contains potential scatterers at different heights than the antennas, we want to show the suitability of a 2D-model, which is computationally much less demanding. The only exception is the inclusion of the floor reflection, which can be incorporated easily.

Naturally, the building geometry restricts the region in which a certain reflection is possible. This is taken into account by computing visibility regions of VAs, which is discussed here. As an example, the geometric visibility of a second-order VA at a position $\mathbf{p}_n$ from an agent position $\mathbf{p}$ can be computed as follows (see also right plot in Fig. 1): First, we test if the line from $\mathbf{p}$ to $\mathbf{p}_n$ intersects the associated second-order reflecting surface in a point $\mathbf{p}_{\mathrm{ref}}$. We also have to make sure, that out of all intersection points of this line with any objects known from the floor plan, $\mathbf{p}_{\mathrm{ref}}$ is the one closest to $\mathbf{p}$, such that the path from the point to the surface is not blocked. If these conditions do not hold, $\mathbf{p}$ is not a valid "target" for this reflection and the VA is not visible. Otherwise, we have to test whether $\mathbf{p}_{\mathrm{ref}}$ is a valid "target" for a first-order reflection at the associated first-order segment of the second-order VA, which can be done using the corresponding first-order VA. This recursive ray-launching could be generalized to higher-order VAs as

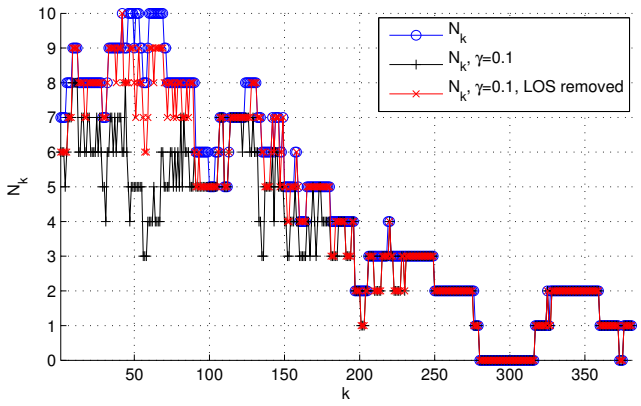

Fig. 2. Number of geometrically visible VAs N_k over the trajectory (blue line) for BS 1. The other lines show the number of significant MPCs from VAs, according to the threshold decision discussed in III-B, with $\gamma = 0.1$. For the black line, the threshold is computed using the full CIR, for the red line, the LOS component has been removed.

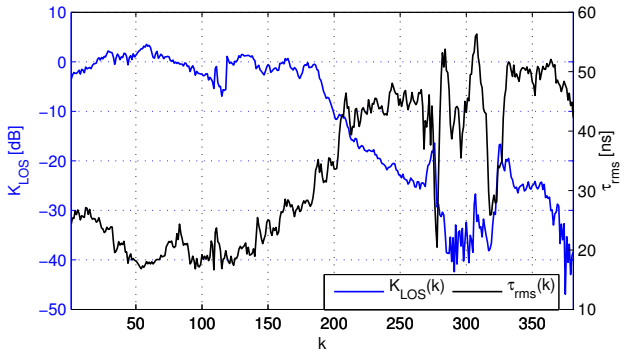

Fig. 3. Instantaneous K-factor w.r.t. the LOS component K_{LOS} and RMS delay spread τ_{rms} over the trajectory for BS 1.

well and is repeated until the base station is reached.

For each VA that is taken into account, the visibility can be precomputed for a sufficiently dense grid of points within the floor plan. Fig.1 contains an example for the computed visibility region of the second-order VA for BS 1, associated to the large window and the adjacent wall. At each step k of the trajectory, the set of expected visible virtual anchors, denoted by $\mathcal{V}_k$, can then simply be looked up in the computed visibilities. The number of expected visible VAs at time-step k is then denoted as $|\mathcal{V}_k| = N_k$. The blue line in Fig. 2 shows N_k for BS 1 over all 381 measured trajectory positions.

III. Channel Analysis Method

A. Channel model and parameters

In the following, we use the channel model

$$h_k(\tau) = \sum_{l=1}^{L} \alpha_{k,l}\delta(\tau - \tau_{k,l}) + \nu_k(\tau) + n_k(\tau) \qquad (1)$$

for the UWB-CIR at time step k, corresponding to position $\mathbf{p}_k$. This model decomposes the channel in three major parts. The first one is a sum over L deterministic, specular reflections, modeled with complex-valued amplitudes $\alpha_{k,l}$ and time delays $\tau_{k,l}$. The signals $\nu_k(\tau)$ and $n_k(\tau)$ model the diffuse scattered parts and the measurement noise, respectively. We expect that at a position $\mathbf{p}_k$, the set of visible VAs $\mathcal{V}_k$ can be used to model a part of the deterministic reflections.

The measurements are the position-variant channel transfer functions (CTF) $H_k(f)$ along the trajectory. An inverse discrete Fourier transform (IDFT) is used for the transformation to time domain. To reduce the leakage effect and to support the MPC cancellation process, which will be described in the next section, we use a Parzen window function in frequency domain prior to the IDFT, hence

$$h_k(\tau) = \frac{1}{N_f} \sum_{f=f_{\min}}^{f_{\max}} H_k(f)W(f)e^{j2\pi f\tau}. \qquad (2)$$

Note that both f and τ are defined as equally spaced discrete values. In time domain, the ideal CIR in (1) is convolved with the impulse response of the window function $w(\tau)$, which can be understood as a pulse shaping step. In (2), $f_{\min}$ and $f_{\max}$ denote upper and lower band edge and N_f is the number of frequency points. The values for τ are selected at a higher resolution as given by the measurement bandwidth, similar to the work in [5]. The upper part of Fig. 5 contains the 381 obtained CIRs $h_k(\tau)$ between mobile agent and BS 1 from our measurements.

Due to the geometric separation of successive agent positions, which is relatively large compared to the wavelength at the upper band edge, no spatial averaging was performed. Hence, we can not use an average power delay profile to compute channel parameters like the RMS-delay spread τ_{rms} and the K-factor with respect to the line-of-sight (LOS)-component [10]. But as these parameters are valuable for the analysis of an UWB channel, we evaluate the instantaneous values of these parameters along the trajectory, as shown in Fig. 3. We note that despite the clear LOS scenario, the K-factor is positive only on the points closest to the base station. This indicates the presence of strong MPCs that can easily bias a localization system whenever the LOS path is blocked. It should also be noted that for positions around $k = 300$, the estimates are unreliable, as this is the region where the agent enters a corridor that is completely hidden from the view of BS 1, c.f. Fig. 1 and 5, hence the CIRs in that region show an extremely low SNR.

B. MPC estimation and cancellation

In order to evaluate the relevance of the MPCs that can be attributed to the VAs, we need to find them in the CIRs and afterwards remove their influence. To this end, we calculate the vector of expected MPC delays at position

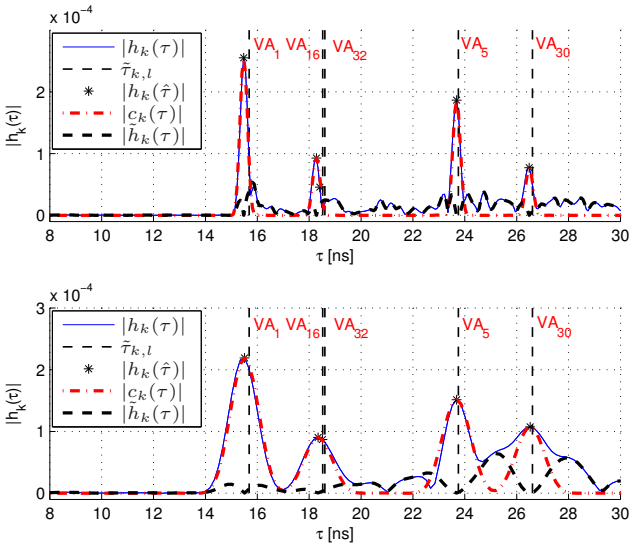

Fig. 4. Example of the MPC-cancellation procedure at position $k = 92$ and BS 1 for a bandwidth of 7.5 GHz (upper plot) and 2 GHz (lower plot), zoomed view. The reflection from the large concrete pillar (VA_{16}) coincides with the floor reflection (VA_{32}).

$\mathbf{p}_k$, corresponding to time step k, as

$$\tilde{\boldsymbol{\tau}}_k = [\tilde{\tau}_{k,1}, \ldots, \tilde{\tau}_{k,N_k}] \quad (3)$$

$$= c^{-1} \cdot [d(\mathbf{p}_1, \mathbf{p}_k), \ldots, d(\mathbf{p}_{N_k}, \mathbf{p}_k)] \quad (4)$$

where the function $d(\cdot)$ denotes the Euclidean distance. We expect that due to uncertainties in the floor plan and/or the placement of the MS, these distances are imperfect. In Fig. 4, the entries of $\tilde{\boldsymbol{\tau}}_k$ are shown as vertical dashed black lines, illustrating some minor geometric errors.

In the sequential cancellation procedure, a cleaned CIR $\tilde{h}_{k,l}(\tau)$ is computed for each MPC, where l is the MPC index with $l \in \{1, \ldots, N_k\}$. The initial cleaned CIR is the measured one, $\tilde{h}_{k,0}(\tau) = h_k(\tau)$. To cancel the l-th MPC, we first calculate an estimate of the true delay of the respective expected MPC $\hat{\tau}_{k,l}$, starting from the corresponding $\tilde{\tau}_{k,l}$. We use a narrow uncertainty window of width $T = 0.5$ ns, or approx. 15 cm, around the expected delays. Within this window, we search for the maximum amplitude of the CIR. The delay at which this maximum is obtained, is our estimate $\hat{\tau}_{k,l}$

$$\hat{\tau}_{k,l} = \arg\max_{\tau \in [\tilde{\tau}_{k,l} - T/2,\ \tilde{\tau}_{k,l} + T/2]} |h_{k,l}(\tau)|. \quad (5)$$

With the estimated $\hat{\tau}_{k,l}$, we generate a template signal for the l-th MPC at position $\mathbf{p}_k$

$$c_{k,l}(\tau) = \frac{\tilde{h}_{k,l}(\hat{\tau}_{k,l})}{N_f} \sum_{f=f_{\min}}^{f_{\max}} W(f) e^{j2\pi f(\tau - \hat{\tau}_{k,l})}. \quad (6)$$

The template consists of the impulse response of the window $W(f)$ (the "pulse shape"), shifted to the estimated delay of the l-th MPC and scaled by the complex amplitude of the current cleaned CIR at the estimated delay. This signal is then used to calculate the CIR cleaned from all up to the l-th MPC

$$\tilde{h}_{k,l}(\tau) = h_{k,l-1}(\tau) - c_{k,l}(\tau) \quad (7)$$

The overall cleaned CIR is then $\tilde{h}_{k,N_k}(\tau)$, and the overall template signal at $\mathbf{p}_k$ consisting of the contributions from expected reflections is simply the summation of the N_k expected MPCs

$$c_k(\tau) = \sum_{l=1}^{N_k} c_{k,l}(\tau). \quad (8)$$

Fig. 4 contains an example for this procedure at $k = 92$ for BS 1, including a comparison of the full measurement bandwidth of 7.5 GHz and the restricted range of 2 GHz (from $6 - 8$ GHz). We can see that the MPC cancellation works well, cancelling the respective MPC without introducing noticeable distortions elsewhere. The higher the bandwidth, the more "local" the cancellation is, i.e. at a lower bandwidth, the estimated MPC (the template signal) also contains other parts of the CIR that happen to be within the window impulse response.

In addition to the geometric mismatch, we also take possible impairments of the visibilities of the VAs into account. For example, at a position $\mathbf{p}_k$, an expected MPC might not be visible (i.e. its amplitude is very low) due to fading or other effects. Another MPC might be visible unexpectedly, e.g. the LOS component is visible longer than predicted by geometry, which is due to diffraction. Hence, we want to determine which of the expected VAs $\mathcal{V}_k$ are actually *significant*. We do this by a threshold decision. The threshold $A_{\gamma,k}$ is defined as a value inbetween the maximum of $|h_k(\tau)|$ and the noise floor, which is computed as the time average of the noise part, $\langle n_k(\tau) \rangle$, where $n_k(\tau)$ is obtained as the part of the CIR before the LOS component

$$A_{\gamma,k} = \gamma \cdot (\max\{|h_k \tau|\} - \langle |n_k(\tau)| \rangle) + \langle |n_k(\tau)| \rangle. \quad (9)$$

An MPC at $\tau = \hat{\tau}_{k,l}$ is then defined as significant, if $|h_k(\hat{\tau}_{k,l})| \geq A_{\gamma,k}$. In strong LOS situations this threshold can be relatively high and restrictive, i.e. it will exclude reflections that are clearly distinguishable from the noisefloor. Therefore we will also use an alternative threshold that is computed in the same way as $A_{\gamma,k}$ in (9), but where the maximum amplitude is taken from the CIR with the LOS component removed.

IV. Performance Results

We performed the described method over the whole trajectory and for all the BSs in order to evaluate the relevance of the part of the UWB channel that can be attributed to the known VAs. Measured CIRs and obtained template signals $c_k(\tau)$ can be seen in Fig. 5 for BS 1 and in Figs. 7-11 for the other BSs. It can be observed that the paths along the trajectory corresponding to VA-caused reflections are matched well. First, the results for BS 1 will be discussed in detail. After that, we will also list the results for the other BSs.

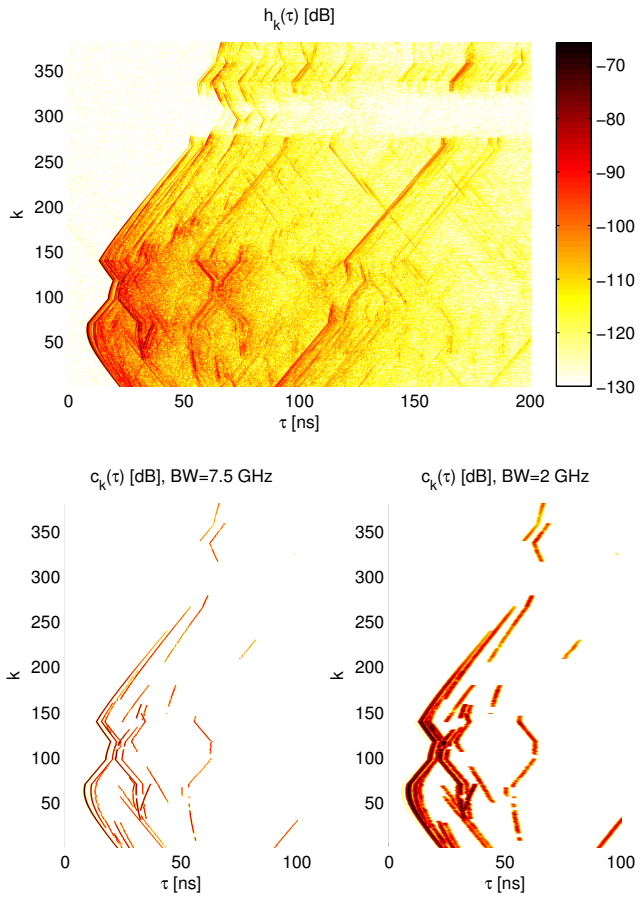

Fig. 5. Measured CIRs between mobile agent and BS 1 over the trajectory (top) and extracted template signals (bottom). Lower left plot shows the templates for the full and lower right plot for the reduced bandwidth. Template plots are zoomed on the τ-axis.

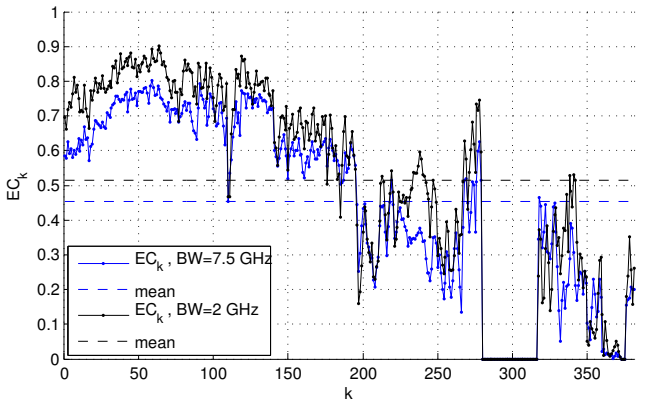

Fig. 6. Energy capture EC_k over the trajectory for the full (blue) and the reduced bandwidth and BS 1. Horizontal dashed lines are corresponding averages.

A. *Detailed results for Base Station 1*

To obtain a quantitative analysis of the results, we use the concept of energy capture [6]. The energy of the CIR at time-step k is defined as

$$\mathrm{E}_k = \int_\tau |h_k(\tau)|^2 d\tau \tag{10}$$

where the integration is performed over the whole measured CIR. With a similar definition for the energy of the cleaned CIR $\tilde{\mathrm{E}}_k$, the energy capture at time-step k is then defined as

$$\mathrm{EC}_k = 1 - \frac{\tilde{\mathrm{E}}_k}{\mathrm{E}_k}. \tag{11}$$

Fig. 6 shows EC_k for BS 1 and both bandwidths over all 381 trajectory positions. We can see that the MPCs caused by the expected VAs can explain a large amount of the signal energy contained in the CIRs. In general, the energy capture is higher for the lower bandwidth. This is explained with the fact that the template of, say, the l-th MPC, i.e. the signal $c_{k,l}(\tau)$, contains not only the corresponding deterministic reflection, but also diffuse parts at that delay as well as possibly other deterministic reflections. As also confirmed qualitatively by Fig. 4, this effect is more pronounced at lower bandwidths, where the duration of the window impulse response $w(\tau)$ is longer. The high bandwidth shows an average energy capture of $47\,\%$ for the entire trajectory, while at the lower bandwidth we achieve $52\,\%$. In roughly the first 180 positions, which according to Fig. 1 might be used as the operating area for this base station, the average energy capture is almost $70\,\%$ for the high bandwidth, and $76\,\%$ for the lower one. We also emphasize the model restriction to second-order reflections as well as to the two-dimensional plane, which does not seem to play a major role, considering the high amount of energy capture that is obtained.

At this point, we also take the significance condition in (9) into account. The black line in Fig. 2 shows the number of significant VA-caused MPCs at a threshold of $\gamma = 0.1$, computed with the maximum amplitude of the full CIR. We can observe that especially in the region of high expected VA density, many of them are considered insignificant. Considering the K-factor in Fig. 3, one can see that this effect is most pronounced in strong LOS situations. Using the alternative threshold that is computed with the LOS-removed CIR, the mean number of significant MPCs in the operating area of BS 1 increases from 5.36 to 6.82 for the high bandwidth, for example (see also Table II). These observations show that the MPCs corresponding to VAs seem to be reliable channel features.

Next, we consider the effect of insignificant MPCs on the energy capture. Fig. 6 has been generated taking all considered VAs into account. However, if EC_k is calculated with just the significant MPCs, we see that at a threshold $\gamma = 0.1$, the maximum penalty in energy capture over all k is only $1.8\,\%$ for the high bandwidth, and $1.9\,\%$ for the low one. This shows that the corresponding insignificant VAs contribute only little energy. Another important observation

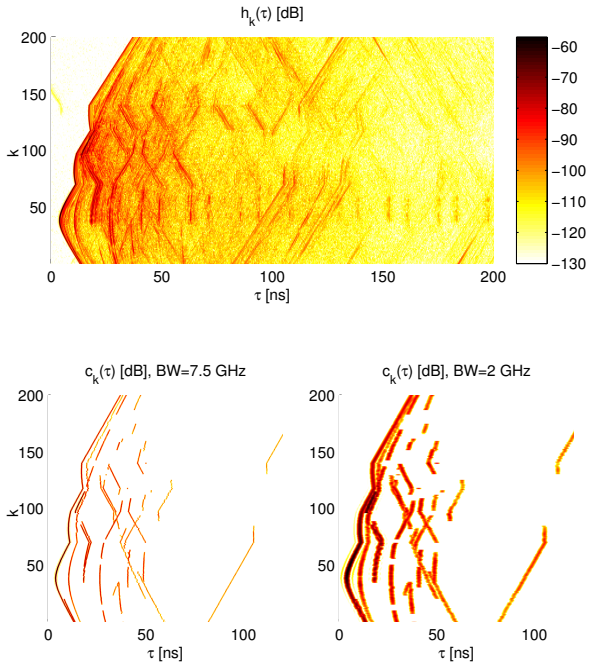

Fig. 7. Measured CIRs between mobile agent and BS 2 over the trajectory (top) and extracted template signals (bottom). Lower left plot shows the templates for the full and lower right plot for the reduced bandwidth. Template plots are zoomed on the τ-axis.

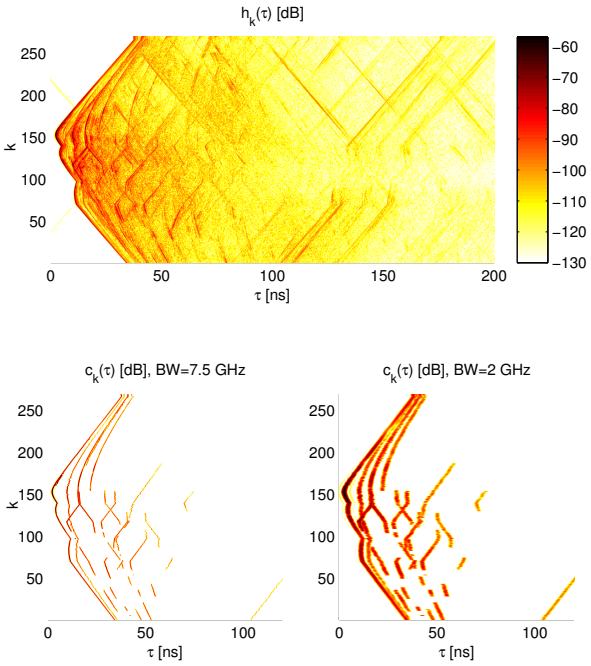

Fig. 8. Measured CIRs between mobile agent and BS 3 over the trajectory (top) and extracted template signals (bottom). Lower left plot shows the templates for the full and lower right plot for the reduced bandwidth. Template plots are zoomed on the τ-axis.

is that, even though some strong reflections are not taken into account due to our model restrictions, there are clearly always more than three significant VAs present in the operating area, which is sufficient for 2D-localization.

B. Results for the other Base Stations

Figs. 7-11 show the CIRs $h_k(\tau)$ as well as the template signals for BSs 2-5 over their corresponding operating areas. In Table II, condensed results are presented. In general, the results are comparable to those of BS 1, i.e. a rather large fraction of the CIR energy can be attributed to the MPCs corresponding to the expected VAs. For BS 5 (see Figs. 1 and 10), considerably less energy capture is achieved. This is a region where the mobile agent is within the small corridor (approx. between positions 270 and 330) consisting of concrete walls and a highly reflective glass door. The environment results in a very rich channel structure and the reflections of order larger than two are not considered in our model. The K-factor in this area is roughly about -5 dB despite the LOS situation and the delay spread is about 40 ns. Nevertheless, a high mean number of significant VAs is achieved.

From all these observations, we conclude that a multipath-aided indoor localization system can indeed expect the presence of deterministic MPCs that correspond to VAs as important features of the channel.

TABLE II
RESULTS FOR ALL BASE STATIONS

BS	mean EC_k		mean N_k, $\gamma = 0.1$		Region
	7.5 GHz	2 GHz	7.5 GHz	2 GHz	
			full CIR / LOS removed		
1	68 %	76 %	5.36 / 6.82	6.09 / 6.91	1 - 180
2	64 %	71 %	4.30 / 6.10	4.58 / 6.20	1 - 200
3	56 %	66 %	5.21 / 6.09	5.31 / 6.06	1 - 270
4	55 %	62 %	4.39 / 4.69	4.47 / 4.73	1 - 381
5	43 %	54 %	5.67 / 6.04	5.86 / 6.04	200 - 381
6	65 %	69 %	3.11 / 4.15	3.23 / 4.23	150 - 381

V. CONCLUSION AND OUTLOOK

We have presented an analysis of a measurement campaign of an indoor UWB channel. A floor plan was used to calculate a set of virtual signal sources plus their expected visibilities. The obtained geometric information was the basis of the channel analysis. We also presented an MPC cancellation method that introduces virtually no artifacts. This work acts as feasibility study for our previously proposed multipath-aided indoor localization algorithms, as it shows that the specular reflections caused by walls and scatter points are relevant features of the channel. Ongoing work includes the refinement of the estimation of the arrival times of the expected MPCs and of course the localization algorithms based on this data.

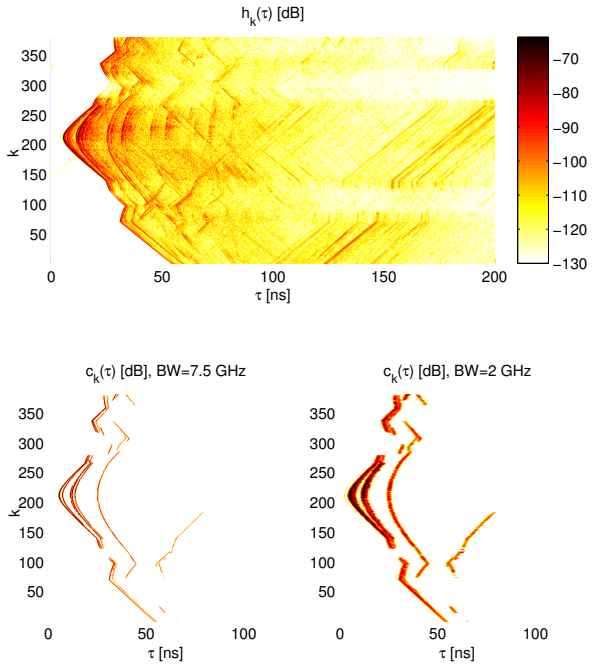

Fig. 9. Measured CIRs between mobile agent and BS 4 over the trajectory (top) and extracted template signals (bottom). Lower left plot shows the templates for the full and lower right plot for the reduced bandwidth. Template plots are zoomed on the τ-axis.

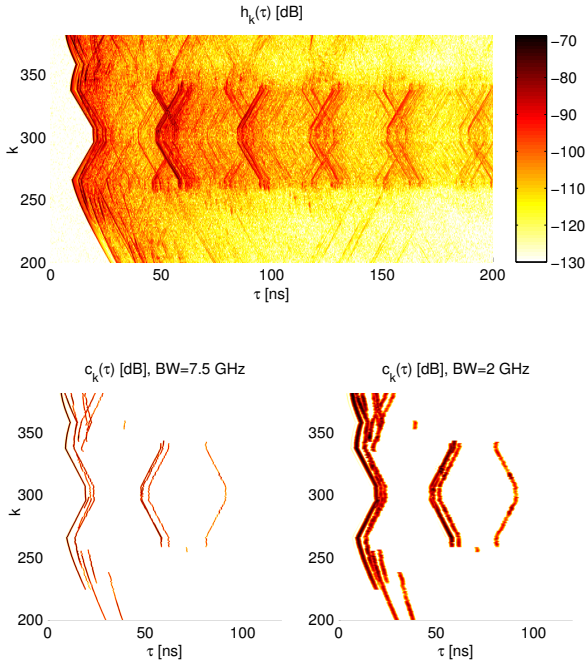

Fig. 10. Measured CIRs between mobile agent and BS 5 over the trajectory (top) and extracted template signals (bottom). Lower left plot shows the templates for the full and lower right plot for the reduced bandwidth. Template plots are zoomed on the τ-axis.

REFERENCES

[1] A. F. Molisch, "Ultra-Wide-Band Propagation Channels," *Proc. IEEE*, vol. 97, no. 2, pp. 353–371, Feb. 2009.

[2] J. Kunisch and J. Pamp, "An ultra-wideband space-variant multipath indoor radio channel model," in *Ultra Wideband Systems and Technologies, 2003 IEEE Conference on*, 16-19 2003, pp. 290 – 294.

[3] P. Meissner, T. Gigl, and K. Witrisal, "UWB Sequential Monte Carlo Positioning using Virtual Anchors," in *Proc. 2010 International Conference on Indoor Positioning and Indoor Navigation, IPIN, Zurich*, 2010.

[4] Y. Shen and M. Win, "On the Use of Multipath Geometry for Wideband Cooperative Localization," in *Global Telecommunications Conference, 2009. GLOBECOM 2009. IEEE*, 30 2009-dec. 4 2009, pp. 1 –6.

[5] T. Santos, J. Karedal, P. Almers, F. Tufvesson, and A. Molisch, "Modeling the ultra-wideband outdoor channel: Measurements and parameter extraction method," *Wireless Communications, IEEE Transactions on*, vol. 9, no. 1, pp. 282 –290, january 2010.

[6] M. Win and R. Scholtz, "Characterization of ultra-wide bandwidth wireless indoor channels: A communication-theoretic view," *Selected Areas in Communications, IEEE Journal on*, vol. 20, no. 9, pp. 1613 – 1627, Dec. 2002.

[7] J. Karedal, S. Wyne, P. Almers, F. Tufvesson, and A. Molisch, "A Measurement-Based Statistical Model for Industrial Ultra-Wideband Channels," *Wireless Communications, IEEE Transactions on*, vol. 6, no. 8, pp. 3028 –3037, 2007.

[8] L. Zwirello, M. Janson, C. Ascher, U. Schwesinger, G. Trommer, and T. Zwick, "Localization in industrial halls via ultra-wideband signals," in *Positioning Navigation and Communication (WPNC), 2010 7th Workshop on*, 2010, pp. 144 –149.

[9] C. Krall, "Signal processing for ultra wideband transceivers," PhD thesis, Graz Univ. of Techn. (Austria), 2008.

[10] A. Molisch, *Wireless Communications*. John Wiley & Sons, 2005.

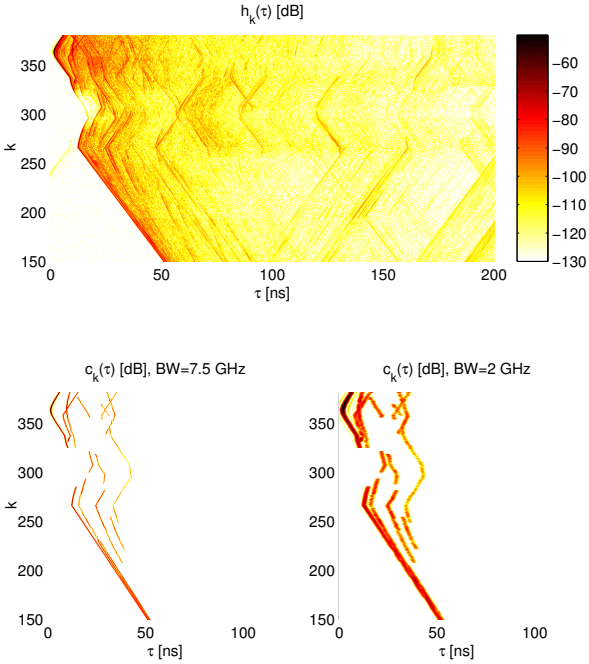

Fig. 11. Measured CIRs between mobile agent and BS 6 over the trajectory (top) and extracted template signals (bottom). Lower left plot shows the templates for the full and lower right plot for the reduced bandwidth. Template plots are zoomed on the τ-axis.